Cavity mode dephasing via the optomechanical interaction with an acoustic environment

Qidong Xu[*] and M. P. Blencowe[†]

Department of Physics and Astronomy, Dartmouth College, Hanover, New Hampshire 03755, USA

We consider an optomechanical system comprising a single cavity mode and a dense spectrum of acoustic modes and solve for the quantum dynamics of initial cavity mode Fock (i.e., photon number) superposition states and thermal acoustic states. The optomechanical interaction results in dephasing without damping and bears some analogy to gravitational decoherence. For a cavity mode locally coupled to a one-dimensional elastic string-like environment or two-dimensional elastic membrane-like environment, we find that the dephasing dynamics depends respectively on the string length and membrane area—a consequence of an infrared divergence in the limit of an infinite-sized string or membrane. On the other hand, for a cavity mode locally coupled to a three-dimensional bulk elastic solid, the dephasing dynamics is independent of the solid volume (i.e., is infrared finite), but dependent on the local geometry of the coupled cavity—a consequence of an ultraviolet divergence in the limit of a "pointlike" coupled cavity. We consider as possible respective realizations for the cavity-coupled one- and two-dimensional acoustic environments an *LC* oscillator capacitively coupled to a partially metalized strip and a cavity light mode interacting via light pressure with a membrane.

I. INTRODUCTION

Cavity optomechanical systems have received considerable attention over the past decades, with applications ranging from the detection of classical gravity waves in the macroscopic domain to the generation and detection of quantum states of mechanical oscillators in the nano-to-mesoscale regimes [1,2]. Most investigations deliberately consider one or at most a few cavity modes interacting similarly with one or at most a few mechanical modes, with notable exceptions including optomechanical interactions between multiple driven bosonic modes and multiple mechanical resonators [3], the consideration of interacting optical and acoustic waves coexisting in bulk, crystalline solids [4], and environment-induced, driven cavity photon blockade and Rabi oscillations via the optomechanical interaction [5].

In this present work, we shall take as our starting point the following Hamiltonian:

$$H = \hbar\Omega\left(a^\dagger a + \frac{1}{2}\right)\left[1 + \sum_i \lambda_i(b_i + b_i^\dagger)\right]$$
$$+ \sum_{i=1}^{N} \hbar\omega_i\left(b_i^\dagger b_i + \frac{1}{2}\right), \quad (1)$$

where a, $a^\dagger$ are the annihilation and creation operators for a cavity mode with frequency Ω, while b_i, $b_i^\dagger$ are the annihilation and creation operators for N mechanical modes. The cavity and mechanical modes are coupled via the standard optomechanical interaction with coupling constant parameters

$\hbar\Omega\lambda_i$. Our particular focus will be on the effective dynamics of the *single* cavity mode system interacting with *many* (i.e., $N \gg 1$) mechanical modes, with the latter viewed as an acoustic, environmental bath for the cavity system. In contrast with the usual quantum Brownian motion model, where the system-bath coupling is bilinear in their respective creation and annihilation coordinates, Hamiltonian (1) does not result in energy damping of the cavity mode system. This is a consequence of the fact that the system Hamiltonian commutes with the interaction Hamiltonian term. On the other hand, dephasing does result for initial superpositions of energy eigenstates of the cavity system; for this reason, Ref. [6] terms Eq. (1) the "phase damped oscillator," and provides a second-order Born-Markov approximated solution to the cavity system reduced density matrix dynamics via a master-equation approach.

As we shall show, the effective dynamics for the cavity system reduced density matrix can in fact be solved *exactly* up to a summation over bath modes, while the latter summation can be carried out approximately for certain bath spectral densities; the method of solution is based on that of Refs. [7,8], which consider a single cavity mode interacting with a single mechanical mode, and which again utilizes the fact that the system and interaction term Hamiltonians commute.

The present work is closely related to Ref. [9], which considers the quantum dephasing and entanglement dynamics of two distinct optical cavity systems, coupled via the optomechanical interaction to a common acoustic field environment.

Our interest in the Hamiltonian (1) and the resulting dephasing dynamics of the cavity mode system reduced state stems from its analog connection with gravitationally induced decoherence [10,11]. In the weak gravitational field regime, the leading-order term in the interaction action involving a scalar matter field $\phi(x)$ system and gravitational metric

_____

[*]qidong.xu.gr@dartmouth.edu
[†]miles.p.blencowe@dartmouth.edu

deviation $h_{\mu\nu}$ from Minkowski space environment takes the form

$$S_I = \sqrt{8\pi G} \int d^4x \, T^{\mu\nu}(\phi) h_{\mu\nu} \tag{2}$$

in natural units $\hbar = c = 1$, where $T^{\mu\nu}(\phi)$ is the scalar field energy-momentum tensor. This interaction term can result in the dephasing of scalar field energy superposition states without energy damping [10,12], just as for the cavity mode quantum dynamics following from Hamiltonian (1) [11]. Comparing the optomechanical interaction Hamiltonian in Eq. (1) with the matter-weak gravity interaction term action (2), the linearly coupled acoustic-phonon field plays the role of the weak graviton field, while the quadratically coupled cavity mode plays the role of the scalar matter field. As discussed in Ref. [11], exploring such optomechanical analogs may shed light on gravitationally induced dephasing dynamics of macroscopic matter-field superposition states.

However, the cavity system dynamics following from Hamiltonian (1) interpreted as modeling cavity optomechanical bath systems is of interest in its own right, particularly the consequences of the acoustic environment spatial dimension and size for the cavity mode energy quantum superposition dephasing dynamics. We shall find that, for one- and two-dimensional (1D and 2D) elastic "string" and "membrane" acoustic environments, respectively, the cavity system dephasing dynamics depends on the geometric size of the environment—a consequence of an infrared (IR) divergence in the limit as the environment size tends to infinity. In contrast, for a bulk, elastic three-dimensional (3D) acoustic environment (which shares the same Ohmic spectral density as for the gravitational wave environment [10]), the cavity dephasing dynamics depends on the size of the optical cavity system embedded within the 3D elastic medium—a consequence of an ultraviolet (UV) divergence in the limit as the size of the cavity tends to zero, i.e., becomes pointlike.

Infrared divergences arising from long-wavelength acoustic flexural modes of membrane-like structures in the infinite-size limit are also encountered in other contexts, for example, the thermal expansion of 2D crystals [13] and atom-membrane surface interactions [14–19].

In Sec. II, we solve for the cavity system reduced density matrix evolution following from the time-dependent Schrödinger equation with Hamiltonian (1) in the Fock state (i.e., photon number) basis for both Ohmic ($s = 1$) and sub-Ohmic ($s = 0, -1$) bath spectral densities [see Eq. (9)], and with the oscillator environment in an initial thermal state. This section extends the analysis of Ref. [11], which considers only the Ohmic case and infinite-sized environment.

In Sec. III, we consider a model cavity-acoustic environment optomechanical system realization involving an *LC* oscillator capacitively coupled to a long, partially metalized, elastic strip and show how this system maps onto the sub-Ohmic $s = -1$ case; several details of the model strip derivation are given in an Appendix. Section IV considers another model system consisting of an optical cavity interacting via light pressure with a large, square elastic membrane [20], which maps onto the sub-Ohmic $s = 0$ case; both Secs. III and IV explore quantitatively by considering, for example, experimentally feasible device parameter values and the cavity mode quantum dephasing dynamics dependence on the acoustic environment size, i.e., the elastic strip length and side dimension of the square membrane. Section V gives a concluding discussion.

II. CAVITY DEPHASING DYNAMICS

Our starting point is the standard single cavity mode optomechanical Hamiltonian (1), but with a bath of mechanical oscillator modes labeled by the index $i = 0, 1, 2, \ldots, N \ggg 1$, instead of the usually considered single-mode case [1]. Hamiltonian (1) neglects cavity-mechanical oscillator bath interaction terms of the form $a^2(b_i + b_i^\dagger)$ and $a^{\dagger 2}(b_i + b_i^\dagger)$, which describe, for example, two photons annihilating and creating a bath phonon ($a^2 b_i^\dagger$), or conversely a bath phonon annihilating and creating two cavity photons ($a^{\dagger 2} b_i$). As we shall see later in Secs. III and IV, such terms can be neglected since the coupling constant λ_i is suppressed for phonon wavelengths much smaller than the cavity size.

We now briefly review the steps for solving the time-dependent Schrödinger equation with Hamiltonian (1) [7,8,11]; further details of the derivation are given in Ref. [11]. We assume that the cavity mode system can be prepared in an initial product state with the bath, the latter of which is assumed to be in a thermal state: $\rho_{\text{initial}} = \rho_c \otimes \rho_{\text{bath}}$. The cavity system initial state is decomposed in terms of the Fock (i.e., number) state basis, $\rho_c = \sum_{n,n'} c_{nn'} |n\rangle\langle n'|$, and the thermal bath state expressed in a coherent-state basis:

$$\rho_{\text{bath}} = \prod_i \frac{1}{\pi(e^{\beta\hbar\omega_i} - 1)} \int d\alpha_i^2 \exp[-|\alpha_i|^2]$$

$$\times (e^{\beta\hbar\omega_i} - 1)]|\alpha_i\rangle\langle\alpha_i|, \tag{3}$$

where $\beta^{-1} = k_B T$, with k_B being Boltzmann's constant and T the bath temperature. Solving first the Schrödinger equation for an initial basis state $|n, \{\alpha_i\}\rangle$ and then tracing out the bath, we obtain for the reduced state of the cavity mode: $\rho_c(t) = \sum_{n,n'} c_{nn'} |n(t)\rangle\langle n'(t)|$, where the time-dependent outer product is [11]

$$|n(t)\rangle\langle n'(t)| = |n\rangle\langle n'| \exp\left\{ -it\left[\Omega(n - n') - (n + n' + 1)(n - n') \sum_i \frac{(\Omega\lambda_i)^2}{\omega_i} \right] \right.$$

$$\left. - i(n + n' + 1)(n - n') \sum_i \left(\frac{\Omega\lambda_i}{\omega_i}\right)^2 \sin(\omega_i t) - 2(n - n')^2 \sum_i \left(\frac{\Omega\lambda_i}{\omega_i}\right)^2 \coth\left(\frac{\beta\hbar\omega_i}{2}\right) \sin^2\left(\frac{\omega_i t}{2}\right) \right\}. \tag{4}$$

Note that this outer product is time independent for $n = n'$, a consequence of the fact that the system oscillator Hamiltonian commutes with the system-bath interaction Hamiltonian.

We now discuss the various terms appearing in Eq. (4). The first imaginary term $-i\Omega(n - n')t$ in the argument of the exponential is just the free cavity oscillator system evolution. The second imaginary term gives rise to a cavity frequency renormalization $\Omega' = \Omega - \sum_i (\Omega\lambda_i)^2/\omega_i$ [from the $(n - n')$ part], as well as an induced Kerr nonlinear self-interaction [from the $(n^2 - n'^2)$ part] in the oscillator Hamiltonian:

$$H = \hbar\Omega a^\dagger a + \hbar\Lambda_{\text{kerr}}(a^\dagger a)^2, \qquad (5)$$

where $\Lambda_{\text{kerr}} = -\sum_i (\Omega\lambda_i)^2/\omega_i$. The third imaginary term cancels the just-described second imaginary term in the short-time limit $t \to 0$, while it decays to zero as t increases due to the oscillating sine term; later below, we give a more quantitative specification of the short- and long-time regimes. Finally, the fourth, real term in the argument of the exponential in Eq. (4) can result in dephasing, causing the off-diagonal terms of the system reduced density operator in the number state basis to decrease with increasing time.

To obtain a more quantitative understanding of the time-dependent behavior of the various terms appearing in the outer product of expression (4), we approximate the discrete sum over the acoustic bath modes with a continuous frequency integral as follows:

$$\pi \sum_i \lambda_i^2 f(\omega_i) \approx C \int_{\omega_1}^\infty d\omega \omega^s f(\omega) e^{-\omega/\omega_u}, \qquad (6)$$

where the function $f(\omega)$ is determined by the ω_i dependence of a given term in the argument of the exponential in Eq. (4) and C is a frequency-independent coupling strength constant; approximation (4) necessarily requires $N \ggg 1$ for a sufficiently dense bath frequency spectrum. Following common convention [21], we term optomechanical cavity-acoustic bath systems with exponent $s = 1$ "Ohmic" and systems with exponent $s < 1$ "sub-Ohmic." The value of the exponent s is determined by the combined frequency dependencies of the acoustic bath mode spectral density and of the optomechanical coupling λ_i. For the concrete example optomechanical model realizations in Secs. III and IV, we will see that the exponents $s = -1$ and $s = 0$ correspond to 1D and 2D acoustic environments, respectively.

Depending on the value of the exponent s and the form of $f(\omega)$, an upper cutoff function with some characteristic cutoff frequency ω_u may be required in order to regularize a possible UV divergence as $\omega \to \infty$. For the model realizations considered in the following sections, an upper cutoff arises naturally through a suppression of the optical-mode system-acoustic bath coupling when the acoustic-phonon wavelength becomes smaller than a characteristic optical cavity system dimension. Note that the functional form of the upper cutoff dependencies for these model examples is not in fact of the same exponential cutoff form as assumed in Eq. (6). Nevertheless, it is still informative to consider the commonly used exponential cutoff since it readily allows closed form analytical expressions for the various summation terms appearing in Eq. (4) approximated as integrals.

Furthermore, a lower-frequency cutoff, which we denote as ω_1 ($\ll \omega_u$) in Eq. (6), may be required depending on the value of the exponent s and the form of the function $f(\omega)$ in order to regularize a possible IR divergence as $\omega \to 0$.

For the model realizations considered in the following sections, a lower frequency cutoff arises naturally as the fundamental, lowest-frequency mode ω_1 of the acoustic environment medium which has a finite size.

Using the integral approximation (6), the two imaginary, induced phase terms in Eq. (4) can be evaluated approximately analytically by expressing them in terms of the incomplete Gamma function $\Gamma(s, z) = \int_z^\infty dx\, x^{s-1} e^{-x}$:

$$it(n + n' + 1)(n - n') \sum_i \frac{\Omega^2\lambda_i^2}{\omega_i}$$
$$\approx it(n + n' + 1)(n - n')\frac{C\Omega^2}{\pi} \int_{\omega_1}^\infty d\omega \omega^{s-1} e^{-\omega/\omega_u}$$
$$= it(n + n' + 1)(n - n')\frac{C\Omega^2\omega_u^s}{\pi}\Gamma\left(s, \frac{\omega_1}{\omega_u}\right), \qquad (7)$$

and

$$-i(n + n' + 1)(n - n') \sum_i \frac{\Omega^2\lambda_i^2}{\omega_i^2} \sin(\omega_i t)$$
$$\approx -i(n + n' + 1)(n - n')\frac{C\Omega^2}{\pi} \int_{\omega_1}^\infty d\omega \omega^{s-2} \sin(\omega t) e^{-\omega/\omega_u}$$
$$= -i(n + n' + 1)(n - n')\frac{C\Omega^2\omega_u^{s-1}}{\pi}$$
$$\times \text{Im}\left[(1 - i\omega_u t)^{1-s}\Gamma\left(s - 1, \frac{\omega_1}{\omega_u}(1 - i\omega_u t)\right)\right]. \qquad (8)$$

The real, induced dephasing term in Eq. (4), with integral approximation (6), can only be expressed analytically in certain time-range limits; we will consider the high-temperature limit defined as $k_B T \gg \hbar/t$ (equivalently $t \gg \beta\hbar$), for which the coth function can be expanded to leading order. The dephasing term can then similarly be expressed approximately in terms of incomplete Gamma functions:

$$-2(n - n')^2 \sum_i \left(\frac{\Omega\lambda_i}{\omega_i}\right)^2 \coth\left(\frac{\beta\hbar\omega_i}{2}\right) \sin\left(\frac{\omega_i t}{2}\right)^2$$
$$\approx -\frac{2C\Omega^2}{\pi}(n - n')^2 \int_{\omega_1}^\infty d\omega \omega^{s-2} \coth\left(\frac{\beta\hbar\omega}{2}\right)$$
$$\times \sin\left(\frac{\omega t}{2}\right)^2 e^{-\omega/\omega_u}$$
$$\approx -\frac{2C\Omega^2}{\pi}(n - n')^2 \int_{\omega_1}^\infty d\omega \omega^{s-2} \frac{2}{\beta\hbar\omega} \sin\left(\frac{\omega t}{2}\right)^2 e^{-\omega/\omega_u}$$
$$= -\frac{2C\Omega^2}{\pi}(n - n')^2 \frac{\omega_u^{s-2}}{\beta\hbar}\left\{\Gamma\left(s - 2, \frac{\omega_1}{\omega_u}\right)\right.$$
$$\left. - \text{Re}\left[(1 - i\omega_u t)^{2-s}\Gamma\left(s - 2, \frac{\omega_1}{\omega_u}(1 - i\omega_u t)\right)\right]\right\}. \qquad (9)$$

In the following three sections, we explore the time dependencies of Eqs. (8) and (9) for the values $s = 1, 0, -1$, respectively. With the presence of the two frequency scales ω_1 and ω_u ($\ggg \omega_1$), we have three different time range scales: the short time limit range $t \ll \omega_u^{-1}$, intermediate time range
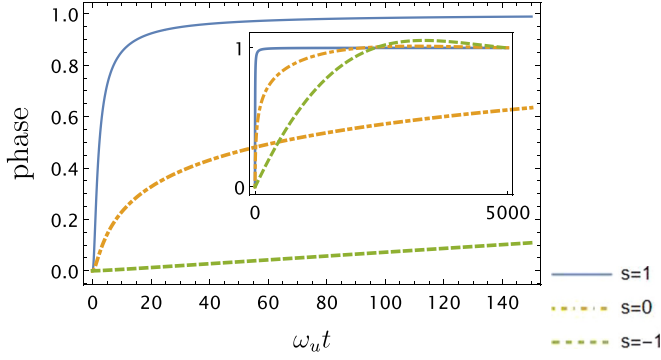
FIG. 1. Sum of the two induced-phase terms (7) and (8) divided by its long time ($t \gg \omega_1^{-1}$) analytical expression as a function of dimensionless time $\omega_u t$, where we set $\omega_1/\omega_u = 0.001$. The inset gives the same normalized phase terms plotted over much longer timescales, indicating the expected approach to 1, hence validating the analytical approximation in the long-time limit.

$\omega_u^{-1} \ll t \ll \omega_1^{-1}$, and the long time limit range $t \gg \omega_1^{-1}$. Note that the high-temperature limit corresponds to requiring $k_B T \gg \hbar \omega_1$ for the intermediate time range. We shall focus below on the intermediate and long time ranges, deriving analytical approximations to the induced phase and dephasing terms by expanding in frequency ratio parameter ω_1/ω_u ($\ll 1$). The numerically evaluated sum of the two induced phase terms (7) and (8) is plotted versus time in Fig. 1, while the numerically evaluated dephasing term integral expression given in the second line of Eq. (9) is plotted versus time in Fig. 2. Both plots are normalized by their corresponding analytical approximations derived below in the $\omega_1 t \rightarrow \infty$ limit, facilitating a check of the analytical approximations in the long-time limit. The analytical approximations derived below for the net induced phase and dephasing terms are summarized in Table I.
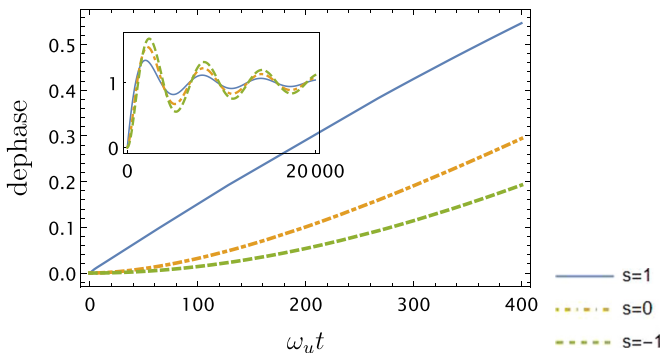

FIG. 2. The numerically evaluated, exact integral expression for the dephasing term given in Eq. (9) divided by its long-time ($t \gg \omega_1^{-1}$) analytical expression as a function of the dimensionless time $\omega_u t$, with $\omega_1/\omega_u = 0.001$ and $\beta \hbar \omega_u = 10$. The inset gives the same normalized dephasing terms plotted over much longer timescales, indicating the expected approach to 1, hence validating the analytical approximation in the long-time limit.

A. Ohmic, $s = 1$ environment case

We begin with the Ohmic case $s = 1$, which corresponds to a 3D acoustic environment medium. The first induced phase term (7) is approximately $it(n + n' + 1)(n - n')\frac{C\Omega^2 \omega_u}{\pi}$, where we have expanded the incomplete Gamma function to leading order using the fact that $\omega_1/\omega_u \ll 1$. We see that this term diverges linearly with the upper frequency cutoff ω_u.

In the intermediate time range ($\omega_u^{-1} \ll t \ll \omega_1^{-1}$), the second induced phase term (8) gives approximately $-i(n + n' + 1)(n - n')\frac{C\Omega^2}{2}$, while for the long time limit ($t \gg \omega_1^{-1}$) we obtain approximately $-i(n + n' + 1)(n - n')\frac{C\Omega^2}{\pi}\frac{\cos(\omega_1 t)}{\omega_1 t}$; in both ranges, the second phase term is small compared with the above first phase term, as remarked previously.

The dephasing term (9) in the high-temperature limit and intermediate time range becomes approximately $-(n - n')^2 C\Omega^2 [\frac{1}{\pi} \ln(\frac{\beta \hbar \omega_u}{2\pi}) + (\beta \hbar)^{-1} t]$, with a leading linear dependence on time t. Note that in order to obtain the correct, logarithmically diverging term in ω_u appearing in the latter approximation, we instead used the exact solution to the dephasing term for $\omega_1 = 0$ derived in Ref. [11]. In the long-time limit ($t \gg \omega_1^{-1}$), the dephasing term (9) becomes approximately $-(n - n')^2 \frac{2C\Omega^2}{\pi \beta \hbar \omega_1}$. Interestingly, this result is finite and independent of time, so that the final, reduced state ρ_c of the cavity system mode will only be partially dephased in the Fock state basis. This is a consequence of the finite-sized volume of the acoustic environment medium, as signified by the nonzero fundamental frequency ω_1 of the medium. We see in the following that partial dephasing also occurs for the $s = 0$ and $s = -1$ cases, again a consequence of the finite dimensions of the corresponding acoustic environments.

In Fig. 2, the approach to the above-described, constant long-time limit displays oscillatory behavior. This arises from the subleading contribution to the dephasing term, which takes the form $-(n - n')^2 \frac{2C\Omega^2}{\pi \beta \hbar \omega_1}\frac{\sin(\omega_1 t)}{\omega_1 t}$. Oscillatory behavior also occurs for the $s = 0$ and $s = -1$ cases, as seen in Fig. 2, arising from similar subleading terms.

B. Sub-Ohmic, $s = 0$ environment case

For the sub-Ohmic $s = 0$ case, which corresponds to a 2D acoustic environment medium, the first induced phase term (7) is approximately $-it(n + n' + 1)(n - n')\frac{C\Omega^2}{\pi}[\ln(\frac{\omega_1}{\omega_u}) + \gamma]$, to leading order in an ω_1/ω_u ($\ll 1$) expansion, where $\gamma \approx 0.5772 \ldots$ is the Euler-Mascheroni constant. Note that this phase term is both logarithmically UV ($\omega_u \rightarrow \infty$) and IR ($\omega_1 \rightarrow 0$) divergent.

For the intermediate time range ($\omega_u^{-1} \ll t \ll \omega_1^{-1}$), the second induced phase term (8) gives approximately $it(n + n' + 1)(n - n')\frac{C\Omega^2}{\pi}[\ln(\omega_1 t) - 1 + \gamma]$. Combining with the above approximate expression for the first phase term, we obtain $it(n + n' + 1)(n - n')\frac{C\Omega^2}{\pi}[\ln(\omega_u t) - 1]$, so that the net induced phase term is logarithmically divergent in the upper frequency cutoff ω_u for the intermediate time range. In the long-time limit ($t \gg \omega_1^{-1}$) the phase term (8) approximates to $-i(n + n' + 1)(n - n')\frac{C\Omega^2}{\pi}\frac{\cos \omega_1 t}{\omega_1^2 t}$. Again, we note that, in the long-time limit, this phase term becomes negligible compared with the first induced-phase term.

TABLE I. Leading order in ω_1/ω_u expansion approximations to the (a) net induced phase terms and (b) dephasing terms in the intermediate time range ($\omega_u^{-1} \ll t \ll \omega_1^{-1}$) and long-time range ($t \gg \omega_1^{-1}$) for Ohmic ($s = 1$) and sub-Ohmic ($s = 0, -1$) bath spectral densities.

(a)	Net induced phase (intermediate time range)	Net induced phase (long time range)
$s = 1$	$it(n + n' + 1)(n - n')\frac{C\Omega^2\omega_u}{\pi}$	$it(n + n' + 1)(n - n')\frac{C\Omega^2\omega_u}{\pi}$
$s = 0$	$it(n + n' + 1)(n - n')\frac{C\Omega^2}{\pi}[\ln(\omega_u t) - 1]$	$-it(n + n' + 1)(n - n')\frac{C\Omega^2}{\pi}[\ln(\omega_1/\omega_u) + \gamma]$
$s = -1$	$it^2(n + n' + 1)(n - n')\frac{C\Omega^2}{4}$	$it(n + n' + 1)(n - n')\frac{C\Omega^2}{\pi\omega_1}$
(b)	Dephasing term (intermediate time range)	Dephasing term (long time range)
$s = 1$	$-(n - n')^2 C\Omega^2\left[\frac{1}{\pi}\ln(\beta\hbar\omega_u/2\pi) + (\beta\hbar)^{-1}t\right]$	$-(n - n')^2\frac{2C\Omega^2}{\pi\beta\hbar\omega_1}$
$s = 0$	$-(n - n')^2\frac{C\Omega^2}{\pi\beta\hbar}\left[\frac{3}{2} - \gamma - \ln(\omega_1 t)\right]t^2$	$-(n - n')^2\frac{C\Omega^2}{\pi\beta\hbar\omega_1^2}$
$s = -1$	$-(n - n')^2\frac{C\Omega^2}{\pi\omega_1\beta\hbar}t^2$	$-(n - n')^2\frac{2C\Omega^2}{3\pi\beta\hbar\omega_1^3}$

The dephasing term (9) in the high-temperature limit and intermediate time range becomes approximately $-(n - n')^2\frac{C\Omega^2}{\pi\beta\hbar}[\frac{3}{2} - \gamma - \ln(\omega_1 t)]t^2$. In contrast with the corresponding $s = 1$ dephasing term given in the previous section, the $s = 0$ dephasing term is not UV divergent, but instead is IR divergent in the limit $\omega_1 \to 0$. In the long-time limit ($t \gg \omega_1^{-1}$), the dephasing term (9) becomes approximately $-(n - n')^2\frac{C\Omega^2}{\pi\beta\hbar\omega_1^2}$.

C. Sub-Ohmic, $s = -1$ environment case

For the sub-Ohmic $s = -1$ case, which corresponds to a 1D acoustic environment medium, the first induced phase term (7) is approximately $it(n + n' + 1)(n - n')\frac{C\Omega^2}{\pi\omega_1}$. In contrast to the corresponding $s = 0$ phase term given in the previous section, this $s = -1$ phase term is IR divergent but not UV divergent.

For the intermediate time range ($\omega_u^{-1} \ll t \ll \omega_1^{-1}$), the second induced phase term (8) gives approximately $-it(n + n' + 1)(n - n')\frac{C\Omega^2}{\pi\omega_1}[1 - \frac{\pi}{4}\omega_1 t]$. Combining with the above approximate expression for the first phase term, we obtain for the net phase term: $it^2(n + n' + 1)(n - n')\frac{C\Omega^2}{4}$, which is neither UV nor IR divergent. In the long-time limit ($t \gg \omega_1^{-1}$) the phase term (8) approximates to $-i(n + n' + 1)(n - n')\frac{C\Omega^2}{\pi}\frac{\cos\omega_1 t}{\omega_1^3 t}$, which becomes negligible compared with the first induced-phase term.

The dephasing term (9) in the high-temperature limit and intermediate time range becomes approximately $-(n - n')^2\frac{C\Omega^2}{\pi\omega_1\beta\hbar}t^2$. Similarly to the corresponding $s = 0$ dephasing term given in the previous section, the $s = -1$ dephasing term, is IR divergent. In the long-time limit ($t \gg \omega_1^{-1}$), the dephasing term (9) becomes approximately $-(n - n')^2\frac{2C\Omega^2}{3\pi\beta\hbar\omega_1^3}$.

III. *LC* CIRCUIT-ELASTIC STRIP MODEL

In this section we consider a model of an *LC* circuit capacitively coupled to a long mechanical strip (Fig. 3), with several details of the derivation given in the Appendix. We show that this model system maps onto the sub-Ohmic $s = -1$ case considered in Sec. II C (although with a different cutoff function and with some modifications to the integral approximation over the bath degrees of freedom). We only consider dephasing, omitting the induced phase terms, i.e.,

cavity frequency renormalization and induced Kerr nonlinearity; the latter phase terms are orders of magnitude smaller than the bare *LC* circuit frequency phase term for the parameters considered later below in this section. We shall furthermore focus primarily on dephasing during the intermediate time range, where most of the dephasing occurs for the considered parameter values.

Referring to Fig. 3, the lower conductor of the capacitor forming the *LC* circuit is assumed fixed, while the upper conductor is a flexing, metalized segment (length ΔL) of a long elastic mechanical strip (length $L \ggg \Delta L$). The transverse width W and thickness T dimensions satisfy $T \ll W \ll L$. The lower capacitor plate is assumed also to have length ΔL and the same width W as the strip, with a small equilibrium vacuum gap between the upper and lower plates: $d \ll W, \Delta L$. The approximate mutual capacitance between the *LC* circuit and the undisplaced strip is approximately $\mathsf{C}_0 = \epsilon_0 W \Delta L/d$ and we denote the circuit inductance as L.

Neglecting motion in the transverse y and longitudinal x directions, we denote the flexing mechanical displacement field of the strip in the transverse z direction by $u_z(x, t)$. For sufficiently large tensile forces F applied at the clamped strip ends such that the elastic bending contribution can be neglected, the Lagrangian for the model, *LC* circuit-mechanical strip system in the resulting string-like limit is as follows:

$$\mathcal{L} = \frac{\rho_m W T}{2}\int_0^L dx\left(\frac{\partial u_z}{\partial t}\right)^2$$
$$- \frac{F}{2}\int_0^L dx\left(\frac{\partial u_z}{\partial x}\right)^2 + \frac{1}{2}\mathsf{C}[u_z]\left(\frac{d\Phi}{dt}\right)^2 - \frac{\Phi^2}{2\mathsf{L}}, \quad (10)$$
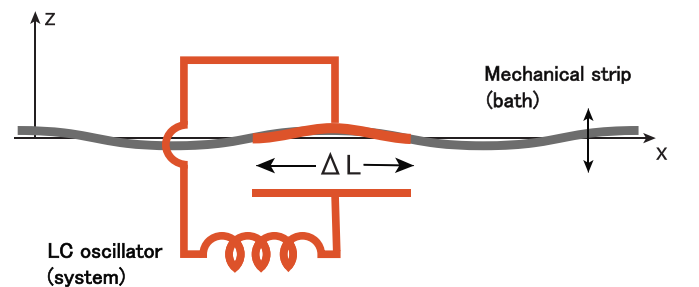

FIG. 3. Effectively 1D optomechanical scheme comprising an *LC* circuit oscillator (system) capacitively coupled to a long oscillating strip with (bath) via a metalized length ΔL.

where $\mathsf{C}[u_z]$ denotes the mechanical displacement-dependent capacitance (with $\mathsf{C}[u_z = 0] \equiv \mathsf{C}_0$, the equilibrium capacitance), Φ is the inductor flux coordinate, and ρ_m is the mechanical strip mass density. Note that Eq. (10) neglects attractive van der Waals-Casimir forces or the possibility of stray, excess charges on the capacitor plates.

Imposing fixed displacement field boundary conditions at the strip ends, $u_z(0) = u_z(L) = 0$ and solving for the free mechanical normal-mode frequencies (see the Appendix), we have

$$\omega_i = \pi i \sqrt{\frac{F}{2mL}}, \quad i = 1, 2, \ldots, \tag{11}$$

with $m = \rho_m WTL/2$ being the effective mass of the mechanical modes. Performing a Legendre transformation to obtain the Hamiltonian from Lagrangian (10), introducing mechanical mode and LC circuit creation and annihilation operators, and expanding the LC circuit frequency $\Omega = 1/\sqrt{LC}$ and creation and annihilation operators to first order in the displacement field u_z, we obtain the optomechanical Hamiltonian (1) after a rotating wave approximation, where the coupling constant λ_i takes the following form (see the Appendix for derivation details):

$$\lambda_i = -\frac{1}{2d}\left(\frac{\hbar}{2m\omega_i}\right)^{1/2} \sin\left(\frac{\pi i}{2}\right) \mathrm{sinc}\left(\frac{\omega_i}{\omega_u}\right), \quad i = 1, 2, \ldots. \tag{12}$$

Here, $\mathrm{sinc}\, x := \sin x / x$ and the upper cutoff frequency is

$$\omega_u = \frac{2}{\Delta L}\sqrt{\frac{FL}{2m}}. \tag{13}$$

Comparing Eq. (13) with the mode-frequency expression (11), we see that the upper cutoff frequency corresponds to the characteristic wavelength $\pi \Delta L$; in the limit where the mechanical mode wavelength becomes much smaller than the capacitor length ΔL, the coupling between the cavity and mechanical strip spatially averages to zero, as expressed by the decaying sinc function appearing in Eq. (12).

With equally spaced, harmonic mode frequencies as given by Eq. (11), we see from Eq. (4) that the dephasing term oscillates, completely vanishing at times $t = 2\pi n/\omega_1$, $n = 0, 1, 2, \ldots$, where from Eq. (11) the lower cutoff frequency is

$$\omega_1 = \pi\sqrt{\frac{F}{2mL}}. \tag{14}$$

We note that such a full rephasing effect is a consequence of having a 1D, harmonic acoustic environment of finite length L with uniformly distributed, discrete modes. This periodic, full rephasing is to be contrasted with the nonzero, long-time-constant dephasing expressions obtained in Sec. II. The origin for this discrepancy is the breakdown of the integral approximation for the mode sums due to the strongly IR divergent nature of the latter appearing in Eq. (4) for the elastic strip model.

An improved integral approximation for the mode sums can be obtained by employing the Euler-Maclaurin series formula to the desired order. In particular, utilizing Eq. (12) for λ_i and the Euler-Maclaurin series approximation to first

order, for example, the integral of the bath spectral density approximation (6) in the large-strip-length-L limit is replaced by

$$\pi \sum_i \lambda_i^2 f(\omega_i) \approx C \int_{\omega_1}^{\infty} d\omega\, \omega^{-1} f(\omega)\mathrm{sinc}^2\left(\frac{\omega}{\omega_u}\right) + C f(\omega_1), \tag{15}$$

where the coupling strength constant is

$$C = \frac{\hbar}{8d^2\sqrt{F\rho_m WT}}, \tag{16}$$

and we have approximated $\mathrm{sinc}(\omega_1/\omega_u) \approx 1$ since $\omega_1 \ll \omega_u$.

Comparing the integral term in Eq. (15) with Eq. (6), we see that the LC circuit-elastic strip (string) model corresponds to the $s = -1$ sub-Ohmic case, but with an upper cutoff of the form $\mathrm{sinc}^2(\omega/\omega_u)$ instead of the previously considered exponential cutoff form $\exp(-\omega/\omega_u)$. Equation (15) gives for the dephasing term in the intermediate time range $(\omega_u^{-1} \ll t \ll \omega_1^{-1})$: $-(n - n')^2 \frac{2C\Omega^2}{\pi \omega_1 \beta \hbar} t^2$, approximately independent of the form of the upper cutoff. Note that the factor of two difference from the corresponding $s = -1$ dephasing expression given in Table I(b) arises from the additional correction term in Eq. (15); including higher-order terms in the Euler-Maclaurin series approximation gives a factor closer to 2.5.

From the ω_1^{-1} dependence of the analytical approximation to the $s = -1$ dephasing term [see Table I(b)], it would seem that the dephasing rate can be made arbitrarily large by progressively increasing the strip length L. However, given that the optomechanical Hamiltonian approximation (1) results from expanding the LC circuit frequency to first order in the mechanical displacement field (i.e., weak-coupling approximation), we necessarily require that mechanical induced fluctuations in the cavity frequency satisfy $\Delta\Omega \ll \Omega$. From Eqs. (1) and (12), and assuming a thermal equilibrium state for the mechanical strip modes, the latter requirement gives (see the Appendix for the derivation details)

$$\sum_{i=1}^{\infty} \frac{\hbar}{8m\omega_i d^2} \sin^2\left(\frac{\pi i}{2}\right)\mathrm{sinc}^2\left(\frac{\omega_i}{\omega_u}\right)\coth\left(\frac{\beta\hbar\omega_i}{2}\right) \ll 1, \tag{17}$$

with ω_i and ω_u given by Eqs. (11) and (13), respectively.

To gain a sense of the dephasing rate magnitudes, we assume example parameter values similar to the silicon nitride vibrating string device of Ref. [22] (although allowing for much longer lengths L than the actual 60 μm), and also assume typical superconducting microwave LC circuit parameters. In particular, we adopt the values $\rho_m = 10^3$ kg/m^3, $F = 10^{-5}$ N, $W = 1$ μm, $T = 0.1$ μm, and $L \gtrsim 1$ cm. For the capacitor dimensions, we assume $\Delta L = 10$ μm and $d = 0.1$ μm. The circuit mode frequency is assumed to be $\Omega/(2\pi) = 5$ GHz, and the acoustic bath temperature is taken to be 50 mK. With these assumed values, we have $\omega_i/(2\pi) = 1.6i\frac{10\,\text{cm}}{L}$ kHz and $\omega_u/(2\pi) = 10$ MHz, giving $\omega_1/\omega_u = 2 \times 10^{-4}\frac{10\,\text{cm}}{L}$. The dephasing term then becomes approximately $-21(n - n')^2 \frac{L}{10\,\text{cm}} \frac{t^2}{\mu\text{s}^2}$ in the intermediate time range $0.02\,\mu\text{s} \ll t \ll 100\frac{L}{10\text{cm}}\,\mu\text{s}$. Thus we see that the phase interference between initial energy superposition states of the LC circuit mode is exponentially suppressed on timescales
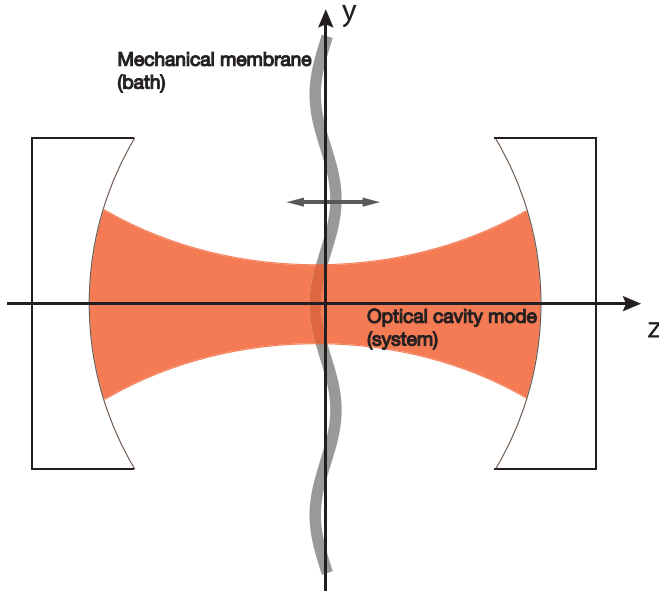
FIG. 4. Optomechanical scheme comprising a cavity light mode (system) trapped between oppositely facing mirrors interacting via light pressure with a thin dielectric membrane of large transverse extent and undergoing transverse flexural oscillations (bath).

of microseconds for few-centimeter-long acoustic strip resonators; we note that such dephasing timescales are roughly of the same order as relaxation and decoherence timescales for superconducting circuits reported in recent experiments [23–25]. Rephasing occurs after a time $\approx 0.6 \frac{L}{10 \text{ cm}}$ msec, neglecting other dephasing mechanisms.

Given that the LC circuit mode frequency satisfies $\Omega = 500\omega_u$, the cavity-mechanical oscillator bath interaction terms of the form $a^2(b_i + b_i^\dagger)$ and $a^{\dagger 2}(b_i + b_i^\dagger)$ may be neglected as discussed in the beginning of Sec. II (corresponding to the rotating wave approximation made in the derivation of the Hamiltonian given in the Appendix). Furthermore, condition (17) on the strip length can be approximated as $L \ll 16\beta d^2 F \approx 2 \times 10^6$ m, which is orders of magnitude longer than in any conceivable circuit optomechanical device operating at cryogenic temperatures, and so the standard optomechanical interaction term in Eq. (1) is well justified. Finally, we note that, e.g., a strip length $L = 10$ cm, the LC-induced phase term $\sum_i \Omega^2 \lambda_i^2/\omega_i$ is approximately 3×10^3 s^{-1}, which is seven orders of magnitude smaller than the bare LC frequency $\Omega = 2\pi \times 5 \times 10^9$ s^{-1}; the LC frequency renormalization and induced Kerr nonlinearity are therefore negligible.

IV. OPTICAL CAVITY-ELASTIC MEMBRANE MODEL

In this section we consider a model of a 3D optical cavity coupled to a large, square mechanical membrane (Fig. 4) [20]. We show that this model system maps onto the sub-Ohmic $s = 0$ case considered in Sec. II C. As in the previous section, we will only consider in detail the dephasing term in the intermediate time range, omitting the induced phase term (i.e., cavity frequency renormalization and induced Kerr nonlinearity).

The cavity-membrane model system can be approximately described by the optomechanical Hamiltonian (1) (see, e.g., Ref. [26]), with the mechanical normal-mode frequencies of the vibrating membrane given by

$$\omega_{i_x i_y} = \pi \sqrt{\frac{\mathcal{F}}{4m} \left(i_x^2 + i_y^2 \right)}, \quad i_x, i_y = 1, 2, \dots, \quad (18)$$

where i_x, i_y are the mode labels marking the spatial dependencies of the modes in the transverse x and y coordinate dimensions of the membrane surface, $\mathcal{F}$ is the tensile force per unit length applied at the clamped membrane edges and m is the effective mass of the mechanical modes:

$$m = \rho_m L^2 T/4, \quad (19)$$

with the membrane having side dimension L and thickness T; the tensile force is here assumed to be sufficiently large that the stretching potential energy dominates over the bending potential energy of the mechanical structure, hence defining the so-called membrane limit.

Restricting to cavity Gaussian beam modes, the cavity normal-mode frequencies are approximately given by the following expression [27]:

$$\Omega_\sigma = \frac{\sigma \pi c}{l} + \frac{2c}{l} \tan^{-1}\left(\frac{l}{2f} \right), \quad \sigma = 1, 2, \dots, \quad (20)$$

where l is the cavity length, f is a length parameter termed the "Rayleigh range" that characterizes the mode beam profile, and c is the speed of light in vacuum.

The optomechanical coupling between the Gaussian beam cavity modes (labeled by σ) and mechanical membrane modes (labeled by i_x, i_y) can be approximated as follows [26]:

$$\lambda_{\sigma, i_x i_y} = (-1)^\sigma \sqrt{\frac{\hbar}{2m\omega_{i_x i_y}}} \frac{(n^2 - 1)T\Omega_\sigma}{lc} \sin\left(\frac{2\Omega_\sigma z_0}{c} \right)$$

$$\times \exp\left(-\frac{\omega_{i_x i_y}^2}{\omega_u^2} \right) \sin\left(\frac{i_x \pi}{2} \right) \sin\left(\frac{i_y \pi}{2} \right), \quad (21)$$

where z_0 is the location of the membrane on the cavity's longitudinal axis, with the membrane positioned such that its center coincides with the center of the cavity mode beam "waist" (i.e., the cavity midpoint with narrowest optical beam width defined as $w_\sigma = \sqrt{2fc/\Omega_\sigma}$), n here denotes the membrane material optical index of refraction, and

$$\omega_u = \sqrt{\frac{8\mathcal{F}}{\rho_m T w_\sigma^2}} \quad (22)$$

is the upper frequency cutoff. Expression (21) assumes that the beam waist w_σ is much smaller than the membrane side dimension L.

Comparing Eq. (22) with the mechanical mode frequency expression (18), we see that the upper cutoff frequency corresponds to a mechanical mode wavelength comparable to the optical beam waist w_σ; in the limit where the mechanical mode wavelength becomes much smaller than the beam waist, the coupling between the cavity and mechanical membrane is exponentially suppressed as the square of the mode frequency.

The integral approximation (6) gives

$$\pi \sum_{i_x,i_y} \lambda_{\sigma,i_x i_y}^2 f(\omega_{i_x i_y}) \approx C \int_{\omega_1}^{\infty} d\omega f(\omega) \exp\left(-\frac{2\omega^2}{\omega_u^2}\right), \quad (23)$$

where, from Eq. (18), the lower cutoff frequency is

$$\omega_1 = \pi \sqrt{\frac{\mathcal{F}}{2m}}, \quad (24)$$

and the coupling strength constant is

$$C = \frac{\hbar}{\mathcal{F}}\left[\frac{(n^2-1)\Omega_\sigma T \sin\left(\frac{2\Omega_\sigma z_0}{c}\right)}{2lc}\right]^2. \quad (25)$$

Comparing the right-hand sides of Eqs. (23) and (6), we see that the optical cavity-elastic membrane model corresponds to the $s = 0$ sub-Ohmic case, but with an upper cutoff of the form $\exp(-2\omega^2/\omega_u^2)$ instead of the previously considered exponential cutoff form $\exp(-\omega/\omega_u)$.

Equation (23) gives for the dephasing term in the intermediate time range $(\omega_u^{-1} \ll t \ll \omega_1^{-1})$ $-(n-n')^2 \frac{1.3 C \Omega_\sigma^2}{\pi \beta \hbar}[\frac{3}{2} - \gamma - \ln(\omega_1 t)]t^2$, approximately independent of the form of the upper cutoff. The factor 1.3 difference with the corresponding $s = 0$ dephasing expression given in Table I(b) accounts for the error in the continuous frequency integral approximation to the discrete sum over membrane modes given by Eq. (23). This factor 1.3 correction was simply determined by trial numerical fitting of the integral approximation over the intermediate time range, since there is no straightforward counterpart to the Euler-Maclaurin formula that gives the correction to the integral approximation of a double sum [28].

To gain a sense of the dephasing rate magnitudes, we assume example parameter values similar to the silicon nitride vibrating membrane device of Ref. [29] (although allowing for much longer membrane side dimensions L than the actual 1 mm). In particular, we adopt the values $n = 2$, $\rho_m = 3.4 \times 10^3$ kg/m^3, $\mathcal{F} = 43$ N/m, $T = 50$ nm, and $L \gtrsim 1$ cm. For the optical mode, we assume a cavity length $l = 3.7$ cm and infrared wavelength $\lambda_\sigma = 1064$ nm, corresponding to frequency $\Omega_\sigma/(2\pi) = 2.8 \times 10^{14}$ Hz and beam waist $w_\sigma = 90$ μm, and suppose that the z_0 location of the membrane in the cavity is chosen such that the factor $|\sin(2\Omega_\sigma z_0/c)| = 1$ in the coupling strength constant expression (25). With these assumed values, we have $\omega_{i_x i_y}/(2\pi) = 2.5(i_x^2 + i_y^2)^{1/2} \frac{10 \text{ cm}}{L}$ kHz and $\omega_u/(2\pi) = 2.5$ MHz, giving $\omega_1/\omega_u = 1.4 \times 10^{-3} \frac{10 \text{ cm}}{L}$. The dephasing term then becomes approximately $-6 \times 10^{-6}(n-n')^2[0.9 - \ln(0.02 \frac{10 \text{ cm}}{L} \frac{t}{\mu s})] \frac{T}{K} \frac{t^2}{\mu s^2}$ in the intermediate time range 0.06 μs $\ll t \ll 45 \frac{L}{10 \text{cm}}$ μs, where $\frac{T}{K}$ refers to the membrane temperature expressed in kelvin. In the long time range $\omega_1^{-1} \ll t$, the dephasing term oscillates strongly but does not completely vanish, in contrast with the strip case considered in Sec. III; due to the nonuniform distribution of the membrane vibrational modes, complete rephasing does not occur.

From the just-derived expression for the dephasing term, we see that it scales approximately quadratically with the membrane edge length L close to the upper limit ω_1^{-1} of the intermediate time range. The resulting estimated dephasing term magnitudes for few centimeter scale-sized membranes are such that the contribution to dephasing of the optical mode

initial Fock state superposition states due to the membrane environment is expected to be negligible compared with that of other sources, such as photon loss from the cavity.

From the form of the coupling strength constant (25), dephasing due to the membrane can also be increased somewhat by reducing the tensile force per unit length $\mathcal{F}$ applied to the membrane edges. However, the membrane approximation assumed in the present investigation eventually breaks down as $\mathcal{F}$ is reduced; the bending potential-energy contribution to the mechanical structure would need to be taken into account, with the structure behaving instead as a so-called plate having a qualitatively different flexural vibration mode spectrum.

Given that the cavity mode frequency satisfies $\Omega_\sigma = 10^8 \omega_u$, the cavity-mechanical oscillator bath interaction terms of the form $a^2(b_i + b_i^\dagger)$ and $a^{\dagger 2}(b_i + b_i^\dagger)$ may be neglected, as discussed in the beginning of Sec. II. In contrast with the cavity-strip system considered in Sec. III, the membrane-induced fluctuations in the cavity mode frequency remain constant with increasing membrane edge length L (with the tensile force per unit length, $\mathcal{F}$, kept fixed) and are negligible compared with the cavity mode frequency, so that there is no upper limit on the membrane edge length for the validity of the standard optomechanical interaction term in Eq. (1). For example, for a membrane edge length $L = 10$ cm, the induced phase term $\sum_{i_x,i_y} \Omega_\sigma^2 \lambda_{\sigma,i_x i_y}^2/\omega_{i_x i_y}$ is approximately 2×10^{-3} s^{-1}, which is eighteen orders of magnitude smaller than the bare LC frequency $\Omega_\sigma = 2\pi \times 2.8 \times 10^{14}$ s^{-1}; the cavity frequency renormalization and induced Kerr nonlinearity are therefore negligible.

V. CONCLUSION

In the present work, we have investigated the quantum dynamics of optomechanical systems in the unusual situation where the mechanical subsystem comprises a dense spectrum of acoustic modes, functioning effectively as an environment for a single optical mode; in particular, the standard optomechanical interaction results in dephasing without dissipation of initial photon number superposition states of the optical mode.

We found that the optical-mode effective dynamics is qualitatively affected by the spatial dimension of the mechanical subsystem, with the dynamics for one-dimensional mechanical environments (which can be realized, for example, as long elastic strings) exhibiting strong power-law infrared divergences, two-dimensional mechanical environments (such as large-area elastic membranes) exhibiting weakly logarithmic infrared and ultraviolet divergences, and three-dimensional mechanical environments (such as large volume elastic solids) exhibiting strong power-law ultraviolet divergences. The infrared divergences are regularized by accounting for the actual, finite size of the mechanical structures, characterized by the lowest mechanical mode frequency ω_1. On the other hand, the ultraviolet divergences are regularized by the suppression of the optomechanical interaction on length scales smaller than the dimensions of the optomechanical interaction region, characterized by a given upper cutoff frequency ω_u $(\gg \omega_1)$.

We furthermore found that the cavity mode effective dynamics depends qualitatively on the timescales considered,

with three different ranges delineated by the inverse frequencies ω_1^{-1} and ω_u^{-1}. Dephasing predominantly occurs during the so-called "intermediate" range $\omega_u^{-1} \ll t \ll \omega_1^{-1}$, with a certain degree of rephasing occurring during the so-called long time range $\omega_1^{-1} \ll t$.

Two possible realizations were considered in some detail, the first being a long elastic strip capacitively coupled to an *LC* circuit over a short segment of the strip, and an optical cavity mode coupled via light pressure to a large area elastic membrane. While the estimated dephasing rates resulting from these realizations are relatively small compared with photon loss rates from the cavities, they nevertheless afford useful model systems for clarifying our understanding of system-environment quantum dynamics for the unusual optomechanical type of interaction, where dephasing occurs without dissipation.

The optomechanical models considered in the present work may be interpreted as analogs for investigating various relativistic quantum information processes, including gravitationally induced dephasing (as briefly discussed in the present work) [10–12] and gravitationally induced entanglement generation [30], discussed in a related paper [9]. By being able to carry out exact analytical calculations in the case of the optomechanical coupling, useful insights may be gained concerning the combined dephasing and entanglement dynamics of gravitationally coupled quantum matter systems [30].

ACKNOWLEDGMENTS

APPENDIX: *LC* CIRCUIT-ELASTIC STRIP MODEL

1. Derivation of the model Hamiltonian

Starting from the Lagrangian in Eq. (10) and performing a Legendre transformation, the Hamiltonian for the model can be found as

$$H = \int_0^L dx \left[\frac{\pi_z(x,t)^2}{2\rho_m WT} + \frac{F}{2} \left(\frac{\partial u_z}{\partial x} \right)^2 \right] + \frac{Q^2}{2\mathsf{C}[u_z]} + \frac{\Phi^2}{2\mathsf{L}},$$
(A1)

where Q and π are the corresponding conjugate momenta for the flux and the displacement field:

$$Q = \frac{\delta L}{\delta \dot{\Phi}},$$
(A2a)

$$\pi_z = \frac{\delta L}{\delta \dot{u}_z}.$$
(A2b)

Since we require that both ends of the strip are fixed with an applied tensile force F, the field u_z then satisfies the boundary condition: $u_z(0) = u_z(L) = 0$, and we can expand it in the normal-mode basis as

$$u_z(x,t) = \sum_{i=1}^{\infty} x_i(t) u_i(x),$$
(A3)

where $u_i(x) = \sin(\frac{\pi i x}{L})$, $i = 1, 2, \ldots$. Substituting Eq. (A3) into Eq. (A1), the strip Hamiltonian takes the independent

harmonic-oscillator form:

$$H = \sum_i \left(\frac{1}{2m} p_i^2 + \frac{1}{2} m \omega_i^2 x_i^2 \right) + \frac{Q^2}{2\mathsf{C}} + \frac{\Phi^2}{2\mathsf{L}},$$
(A4)

where $p_i = m \frac{dx_i}{dt}$, m is the mechanical mode effective strip mass:

$$m = \tfrac{1}{2} \rho_m WTL,$$
(A5)

and ω_i is the normal-mode frequency:

$$\omega_i = \frac{\pi i}{L} \sqrt{\frac{F}{\rho_m WT}}.$$
(A6)

Quantization proceeds by promoting the coordinates Φ, x_i and their conjugate momenta into operators and imposing the usual commutation rules. Introducing the creation and annihilation operators defined by

$$Q = -i \left(\frac{\hbar}{2} \sqrt{\frac{\mathsf{C}}{\mathsf{L}}} \right)^{1/2} (a - a^{\dagger}),$$
(A7a)

$$\Phi = \left(\frac{\hbar}{2} \sqrt{\frac{\mathsf{L}}{\mathsf{C}}} \right)^{1/2} (a + a^{\dagger}),$$
(A7b)

$$x_i = \left(\frac{\hbar}{2m\omega_i} \right)^{1/2} (b_i + b_i^{\dagger}),$$
(A7c)

$$p_i = -i \left(\frac{m\hbar\omega_i}{2} \right)^{1/2} (b_i - b_i^{\dagger}),$$
(A7d)

the Hamiltonian simplifies to

$$H = \hbar\Omega \left(a^{\dagger}a + \frac{1}{2} \right) + \sum_n \hbar\omega_i \left(b_i^{\dagger}b_i + \frac{1}{2} \right),$$
(A8)

where $\Omega = 1/\sqrt{\mathsf{LC}}$; both Ω and the creation and annihilation operators $a^{\dagger}$, a are functionals of the elastic strip displacement field u_z through their dependence on the strip capacitance $\mathsf{C}[u_z]$.

2. Derivation of the coupling constant λ_i

To obtain the optomechanical coupling between the *LC* circuit and the mechanical mode, we expand Ω to first order in the normal-mode displacement coordinates:

$$\Omega \approx \Omega_0 + \sum_i \frac{\partial \Omega}{\partial x_i} \bigg|_{x_i=0} x_i$$

$$= \frac{1}{\sqrt{\mathsf{LC}_0}} - \sum_i \frac{\Omega_0}{2\mathsf{C}_0} \frac{\partial \mathsf{C}}{\partial x_i} \bigg|_{x_i=0} \left(\frac{\hbar}{2m\omega_i} \right)^{1/2} (b_i + b_i^{\dagger})$$

$$= \frac{1}{\sqrt{\mathsf{LC}_0}} + \sum_i \Omega_0 \lambda_i (b_n + b_n^{\dagger}),$$
(A9)

where we define the coupling constant λ_i through the last line of Eq. (A9). To be consistent with this linear approximation, we must also expand to first order the *LC* oscillator creation and annihilation operators in the displacement coordinates. This results in additional interaction terms of the form $a^2(b_i + b_i^{\dagger})$ and $a^{\dagger 2}(b_i + b_i^{\dagger})$, which are usually neglected through the

so-called "rotating wave approximation" [31], hence resulting in the Hamiltonian (1).

To determine the explicit form of the coupling constant λ_i, we require the mode coordinate derivative of the capacitance. Assuming a positive charge $+Q$ placed on the upper conductor of the capacitor and a negative charge $-Q$ placed on the lower conductor, the electric field between the conductors can be found by solving the Laplace equation for the electric potential ϕ:

$$\frac{\partial^2 \phi}{\partial z^2} = 0, \tag{A10}$$

where we neglect edge effects and approximate the electric field to be along the z direction within the capacitor. With the lower strip at $z = -d$ and upper strip at $z = u_z(x)$, the boundary conditions for the electric potential are

$$\phi(x, z = -d) = V_l, \tag{A11a}$$

$$\phi(x, z = u_z(x)) = V_u, \tag{A11b}$$

where V_l, V_u are the voltages on the lower and upper conductors. Since the displacement field u_z is assumed to be much smaller than d_0, we can write the electric potential as a series expansion $\phi = \phi^{(0)} + \phi^{(1)} + \cdots$. Substituting this series into the boundary conditions (A11), we have

$$\phi^{(0)}(x, -d) = V_l, \tag{A12a}$$

$$\phi^{(0)}(x, 0) = V_u, \tag{A12b}$$

and

$$\phi^{(1)}(x, -d) = 0, \tag{A13a}$$

$$\phi^{(1)}(x, 0) = -\frac{\partial \phi^{(0)}(x, z)}{\partial z}\bigg|_{z=0} u_z(x). \tag{A13b}$$

Solving the Laplace equation for $\phi^{(0)}$ and $\phi^{(1)}$ and taking the gradient, we obtain the electric field:

$$\begin{aligned}
\mathbf{E} &= -\nabla(\phi^{(0)} + \phi^{(1)}) \\
&= -\frac{\Delta V}{d}\left(1 - \frac{u_z(x)}{d}\right)\hat{z},
\end{aligned} \tag{A14}$$

where $\Delta V = V_u - V_l$. To determine the relationship between the charge Q and the voltage difference ΔV, we apply Gauss's law to a surface that just encloses the upper surface charge and we have:

$$\begin{aligned}
Q &= \frac{\epsilon_0 \Delta V W \Delta L}{d} - \frac{\epsilon_0 \Delta V W}{d^2}\int_{\frac{L-\Delta L}{2}}^{\frac{L+\Delta L}{2}} dx\, u_z(x) \\
&= \mathsf{C}_0 \Delta V - \frac{\mathsf{C}_0}{\Delta L d}\int_{\frac{L-\Delta L}{2}}^{\frac{L+\Delta L}{2}} dx\, u_z(x).
\end{aligned} \tag{A15}$$

With Eq. (A15), we have the expression for the capacitance:

$$\mathsf{C} = \frac{Q}{\Delta V} = \mathsf{C}_0 - \frac{1}{\Delta L d}\int_{\frac{L-\Delta L}{2}}^{\frac{L+\Delta L}{2}} dx\, u_z(x). \tag{A16}$$

Using the expansion for the displacement field Eq. (A3) and substituting Eq. (A16) into Eq. (A9), we find

$$\lambda_i = -\frac{L}{\pi i d \Delta L}\,\mathrm{sinc}\left(\frac{\pi i \Delta L}{2L}\right)\sin\left(\frac{\pi i}{2}\right)\left(\frac{\hbar}{2m\omega_i}\right)^{1/2}, \tag{A17}$$

where $\mathrm{sinc}\, x := \sin x / x$. Expressing the coupling constant λ_i in a frequency-dependent form, we finally have the expression for λ_i given by Eq. (12):

$$\lambda_i = -\frac{1}{2d}\,\mathrm{sinc}\left(\frac{\omega_i}{\omega_u}\right)\sin\left(\frac{\pi i}{2}\right)\left(\frac{\hbar}{2m\omega_i}\right)^{1/2}, \tag{A18}$$

where the upper cutoff frequency is

$$\omega_u = \frac{2}{\Delta L}\sqrt{\frac{F}{\rho_m W T}}. \tag{A19}$$

3. Derivation of the strip-length condition

From Eq. (A9), we have

$$\Omega \approx \Omega_0 + \sum_i \Omega_0 \lambda_i \left(\frac{2m\omega_n}{\hbar}\right)^{1/2} x_n. \tag{A20}$$

Requiring that the variance of the capacitor frequency to be small compared with the square of its bare frequency Ω_0^2, we have

$$\left\langle\left(\sum_i \Omega_0 \lambda_i \left(\frac{2m\omega_i}{\hbar}\right)^{1/2} x_i\right)^2\right\rangle \ll \Omega_0^2. \tag{A21}$$

For a thermal harmonic oscillator with mass m and frequency ω, the variance for x is

$$\langle x^2 \rangle = \frac{\hbar}{2m\omega}\coth\left(\frac{\beta\hbar\omega}{2}\right), \tag{A22}$$

so that Eq. (A21) becomes

$$\sum_i \lambda_i^2 \coth\left(\frac{\beta\hbar\omega_i}{2}\right) \ll 1, \tag{A23}$$

where we use the fact that different mechanical modes are statistically independent. Substituting the expression (12) for λ_i into Eq. (A21), we obtain condition (17):

$$\sum_i \frac{\hbar}{8m\omega_i d^2}\,\mathrm{sinc}^2\left(\frac{\omega_i}{\omega_u}\right)\sin^2\left(\frac{\pi i}{2}\right)^2\coth\left(\frac{\beta\hbar\omega_i}{2}\right) \ll 1. \tag{A24}$$

[1] M. Aspelmeyer, T. J. Kippenberg, and F. Marquardt, Rev. Mod. Phys. **86**, 1391 (2014).

[2] W. P. Bowen and G. J. Milburn, *Quantum Optomechanics* (CRC Press, Boca Raton, 2015).

[3] D. E. Bruschi, J. Math. Phys. **60**, 062105 (2019).

[4] W. H. Renninger, P. Kharel, R. O. Behunin, and P. T. Rakich, Nat. Phys. **14**, 601 (2018).

[5] Y. Minoguchi, P. Kirton, and P. Rabl, arXiv:1904.02164.

[6] C. W. Gardiner and P. Zoller, *Quantum Noise: A Handbook of Markovian and Non-Markovian Quantum Stochastic Methods*

with Applications to Quantum Optics, 2nd ed., Springer Series in Synergetics (Springer, Berlin, New York, 2000).

[7] S. Bose, K. Jacobs, and P. L. Knight, Phys. Rev. A **56**, 4175 (1997).

[8] S. Bose, K. Jacobs, and P. L. Knight, Phys. Rev. A **59**, 3204 (1999).

[9] Q. Xu and M. P. Blencowe, arXiv:2110.13278 (2021).

[10] M. P. Blencowe, Phys. Rev. Lett. **111**, 021302 (2013).

[11] Q. Xu and M. P. Blencowe, arXiv:2005.02554 (2020).

[12] C. Anastopoulos and B. L. Hu, Classical Quantum Gravity **30**, 165007 (2013).

[13] K. H. Michel, S. Costamagna, and F. M. Peeters, Phys. Status Solidi B **252**, 2433 (2015).

[14] D. P. Clougherty, Phys. Rev. B **90**, 245412 (2014).

[15] S. Sengupta, V. N. Kotov, and D. P. Clougherty, Phys. Rev. B **93**, 235437 (2016).

[16] D. P. Clougherty and S. Sengupta, Phys. Rev. A **95**, 052110 (2017).

[17] D. P. Clougherty, Phys. Rev. B **96**, 235404 (2017).

[18] S. Sengupta and D. P. Clougherty, Phys. Rev. B **96**, 035419 (2017).

[19] S. Sengupta, Phys. Rev. B **100**, 075429 (2019).

[20] J. D. Thompson, B. M. Zwickl, A. M. Jayich, F. Marquardt, S. M. Girvin, and J. G. E. Harris, Nature (London) **452**, 72 (2008).

[21] A. J. Leggett, S. Chakravarty, A. T. Dorsey, M. P. A. Fisher, A. Garg, and W. Zwerger, Rev. Mod. Phys. **59**, 1 (1987).

[22] R. Schilling, H. Schütz, A. H. Ghadimi, V. Sudhir, D. J. Wilson, and T. J. Kippenberg, Phys. Rev. Appl. **5**, 054019 (2016).

[23] M. Reagor, W. Pfaff, C. Axline, R. W. Heeres, N. Ofek, K. Sliwa, E. Holland, C. Wang, J. Blumoff, K. Chou, M. J. Hatridge, L. Frunzio, M. H. Devoret, L. Jiang, and R. J. Schoelkopf, Phys. Rev. B **94**, 014506 (2016).

[24] K. X. Wei, I. Lauer, S. Srinivasan, N. Sundaresan, D. T. McClure, D. Toyli, D. C. McKay, J. M. Gambetta, and S. Sheldon, Phys. Rev. A **101**, 032343 (2020).

[25] H. Zhang, S. Chakram, T. Roy, N. Earnest, Y. Lu, Z. Huang, D. K. Weiss, J. Koch, and D. I. Schuster, Phys. Rev. X **11**, 011010 (2021).

[26] M. J. Underwood, Ph.D. thesis, Yale University, 2016 (unpublished).

[27] G. Brooker, *Modern Classical Optics*, Oxford Master Series in Physics No. 8 (Oxford University Press, Oxford, New York, 2003).

[28] J. Guo and Y. Liu, Commun. Theor. Phys. **73**, 075002 (2021).

[29] M. Underwood, D. Mason, D. Lee, H. Xu, L. Jiang, A. B. Shkarin, K. Børkje, S. M. Girvin, and J. G. E. Harris, Phys. Rev. A **92**, 061801(R) (2015).

[30] S. Bose, A. Mazumdar, G. W. Morley, H. Ulbricht, M. Toroš, M. Paternostro, A. A. Geraci, P. F. Barker, M. S. Kim, and G. Milburn, Phys. Rev. Lett. **119**, 240401 (2017).

[31] C. K. Law, Phys. Rev. A **51**, 2537 (1995).